Modeling and Analysis for the GPS Pseudo-Range Observable

WEIHUA ZHUANG, Member IEEE
University of Waterloo
Canada

JAMES TRANQUILLA, Senior Member IEEE
University of New Brunswick
Canada

In this paper, a digital system for the Global Positioning System (GPS) pseudo-range observable is modeled and analyzed theoretically. The observable is measured in a GPS receiver by accurately tracking the pseudorandom noise (PRN) code phase of the input GPS signal using a digital energy detector and a digital delay lock loop (DDLL). The following issues are presented: 1) mathematical modeling of the digital PRN code acquisition and tracking system, 2) the closed-form expression derivation for the detection and false-alarm probabilities of the acquisition process and for the variance of code phase tracking error, and 3) the linear and nonlinear performance analysis of the DDLL for optimizing the receiver structures and parameters with tradeoff between the tracking errors due to receiver dynamics and due to input noise.

Manuscript received August 7, 1993; revised February 14, 1994.

IEEE Log No. T-AES/31/2/08016.

Authors' addresses: W. Zhuang, Department of Electrical and Computer Engineering, University of Waterloo, Waterloo, Ontario, Canada N2L 3G1; J. Tranquilla, Department of Electrical Engineering, University of New Brunswick, Fredericton, NB, Canada E3B 5A3.

I. INTRODUCTION

The Global Positioning System (GPS) pseudo-range is the raw range (from a GPS satellite to a GPS receiver) measurement before applying signal propagation delay corrections and before having determined time bias of the satellite and receiver clocks. With the pseudo-range measurements from at least four satellites, the three-dimensional coordinates and clock bias correction of the receiver can be obtained. The pseudo-range is measured in a GPS receiver by evaluating the GPS signal propagation time delay from the satellite, based on the time information (of the satellite clock) carried by the C/A (clear/acquisition) code sequence and P (precision) code sequence modulated on the two L band (L1 and L2) carriers [1]. Both C/A code and P code are pseudorandom noise (PRN) code. Each channel of the GPS receiver generates an identical PRN code to synchronize the PRN code of the input GPS signal from the satellite. Once the receiver locally generated PRN code is matched with the PRN code of the input satellite signal, the input PRN code phase is known, from which the satellite clock can be derived. The pseudo-range time delay is estimated by calculating the time difference between the satellite clock and the receiver clock. The pseudo-range can then be determined by multiplying the pseudo-range time delay by the electromagnetic wave propagation velocity. The synchronization between the two PRN codes is accomplished in two steps: 1) code phase acquisition process, which reduces the uncertainty interval of the input code phase to less than one code chip width, and 2) code phase tracking process, which accurately tracks the variations of the incoming code phase and keeps the code phase alignment error within an allowable limit. Research on the PRN code acquisition and tracking of analog systems has been carried on for many years. Serial search techniques are by far the most commonly used to achieve the initial coarse synchronization for low input carrier-to-noise density ratio (C/N_0) environments, the simplest of which is the fixed dwell time method [2–5]. Analog delay lock loops have been used in spread spectrum systems for PRN code accurate synchronization [6–9].

Highly digitized receiver structures are becoming increasingly common in GPS receiver designs. Compared with an analog GPS receiver, a digital GPS receiver has advantages of higher positioning accuracy (due to its robustness to input noise), smaller size, lighter weight and higher power efficiency. Therefore, we focus our attention here on the modeling and analysis of a digital system for measuring the GPS pseudo-range. The object here is to study the code acquisition and tracking processes of a digital GPS receiver. In Section II, a code phase acquisition scheme is modeled and investigated with a digital energy detector, serial search strategies and

double-dwell cell logic. The detection and false-alarm probabilities of the acquisition process are derived. In Section III, a digital delay lock loop (DDLL) is modeled and analyzed for the input code phase fine tracking after the coarse alignment between the two codes is verified. Based on the power spectral density analysis of both input signal and noise, the closed-form expression of the variance of the code phase tracking error due to input noise is obtained. The linear and nonlinear performance of the DDLL is studied for optimizing the loop parameters with tradeoff between the code phase tracking errors due to system dynamics and due to input noise. The conclusions on the pseudo-range measurement performance are presented in Section IV.

II. PRN CODE PHASE ACQUISITION

Serial-search techniques are used because of the low (C/N_0) values of the input GPS signals. For the L1-C/A channel which processes the C/A code signal modulated on the L1 carrier, the acquisition process includes both initial synchronization of the C/A code phase and coarse estimation of the Doppler frequency shift. Sweeping of the uncertainty range of the input code phase and Doppler shift is performed with discrete steps in a digital baseband processor (DBP) of the receiver. The uncertainty region of the potential input code phase and Doppler shift is divided into two-dimensional searching cells. The reference code phase and frequency of each cell are detected by attempting to despread the received signal. If the estimated code phase and Doppler shift are close to the actual values, despreading will occur and be detected; otherwise, no despreading will be sensed and the local code generator and carrier numerically controlled oscillator (NCO) will step to a new code phase delay and/or a new Doppler shift estimate for evaluation until the coarse synchronization on both code phase and carrier frequency is obtained. Because of the uniform uncertainty of the input C/A code phase over the whole code period, it is appropriate to use a straight-line search for the code phase acquisition. If *a priori* information of the Doppler shift is not available, the same strategy is used for the search of the Doppler shift, otherwise a nonuniform distribution of the Doppler shift over the uncertainty region is assumed, with higher probability density near the initial estimate value and lower probability density far away from the estimate value. The search thus proceeds in an expanding-window pattern starting from the cell containing the initial Doppler shift estimate and advancing in both directions. For the acquisitions of the P code modulated on the L1 carrier (L1-P) and on the L2 carrier (L2-P), the initial estimate of code phase is obtained from the L1-C/A code phase and the input hand-over-word (HOW) information of the GPS navigation message. The estimation is accurate to a few P code chips. Because of the *a priori* information, the expanding-window search is used. The accurate code phase tracking of the L1-C/A channel provides the P channels with accurate Doppler shifts, which leaves little uncertainty in the frequency domain for the P code acquisitions.

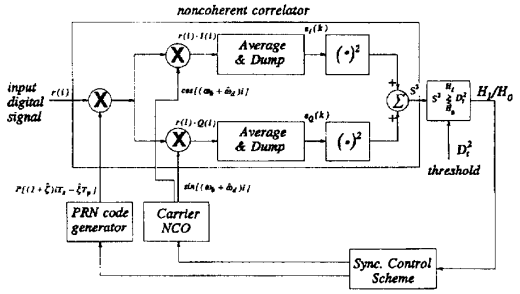

Fig. 1. Block diagram of code acquisition system.

The code phase acquisition system (at baseband) consists of a noncoherent code correlator, a digital phase alignment detector and synchronization control logic, as shown in Fig. 1. Some parameters are defined as follows.

A	Amplitude of received signal
T_s	Sampling duration
T_p	PRN code chip width
f_b	Baseband carrier frequency (which is not chosen to be zero due to the uncertainty of the Doppler frequency shift)
f_d	Doppler frequency shift of the input signal
f_L	RF frequency, which is equal to 1575.42 MHz and 1227.60 MHz for the L1 and L2 carrier signals, respectively
ϕ	Carrier phase (ϕ_0: the initial carrier phase)
R_0	PRN code rate when the Doppler shift is equal to zero, which is 1.023 Mbps for C/A code and 10.23 Mbps for P code
R	PRN code rate when Doppler shift is not equal to zero
τ	PRN code phase delay in second with respect to the GPS system time
$P[x]$	± 1 valued PRN code signal with time-variant code phase x.

The Doppler frequency shift due to the relative movement between the satellite and the receiver has two-fold impact on the received signal: 1) carrier frequency offset—the received carrier signal frequency is equal to $f_L + f_d$; 2) PRN code chip rate offset—because the PRN code is modulated on the carrier signal, the code rate R of the received signal is equal to $(1 + \zeta)R_0$, where ζ $(= f_d/f_L)$ is the code rate offset normalized to R_0. Therefore, the code phase of the received signal, at the ith sample, is

$$x_i = (1 + \zeta)iT_s - \xi T_p \tag{1}$$

where $\xi = \tau/T_p$ is the code phase delay normalized to code chip width T_p. The baseband received signal can be represented as

$$r(i) = A \cdot P[(1+\zeta)iT_s - \xi T_p] \cdot \cos[(\omega_b + \omega_d)i + \phi_0] + n(i) \quad (2)$$

where $\omega_b = 2\pi f_b T_s$ and $\omega_d = 2\pi f_d T_s$ are the digital radian frequencies corresponding to the baseband carrier frequency f_b and Doppler shift f_d, $n(i)$ is the equivalent input Gaussian noise at baseband. If the signal parameters are assumed to be constant quantities (although unknown) over a sufficiently short observation interval, one possible approach to the statistical estimation of code phase delay τ (or ξ equivalently) and code chip rate R (or ω_d) is to seek the maximum-likelihood estimate (MLE) $\hat{\xi}_{\mathrm{ML}}$ of ξ and $\hat{\omega}_{\mathrm{dML}}$ of ω_d. It has been shown that the MLEs of ξ and ω_d are those values of $\hat{\xi}$ and $\hat{\omega}_d$ which simultaneously maximize the likelihood function [10]

$$L(\hat{\xi},\hat{\omega}_d) \triangleq \frac{1}{N_0}\left|\sum_{i=0}^{N-1} r(i)\cdot P[(1+\hat{\zeta})iT_s - \hat{\xi}T_p]\cdot e^{j(\omega_b+\hat{\omega}_d)i}\right| \quad (3)$$

where $\hat{\zeta}$, $\hat{\xi}$ and $\hat{\omega}_d$ are the estimates of ζ, ξ and ω_d, N_0 is the one-side power spectral density of the input noise $n(i)$. In the above equation, $\hat{\zeta}$ has a unique relationship with $\hat{\omega}_d$ (i.e. $\hat{\zeta} = \hat{\omega}_d/2\pi T_s f_L$), so that $L(\hat{\xi},\hat{\omega}_d)$ is a two-dimensional function of ξ and ω_d. In order to obtain the MLE of ξ and ω_d, the receiver local signal generator generates the following in-phase (I) and quadrature (Q) signals to correlate the input signal

$$\begin{aligned} I(i) &= P[(1+\hat{\zeta})iT_s - \hat{\xi}T_p]\cdot\cos[(\omega_b+\hat{\omega}_d)i] \\ Q(i) &= P[(1+\hat{\zeta})iT_s - \hat{\xi}T_p]\cdot\sin[(\omega_b+\hat{\omega}_d)i]. \end{aligned} \quad (4)$$

The "Average & Dump" function block in Fig. 1 averages its input data, i.e. $r(i)\cdot I(i)$ and $r(i)\cdot Q(i)$ for the I and Q channels, respectively, with each average (correlation) interval equal to $T_n = N\cdot T_s$ (where N is an integer). We define normalized code phase estimation error as $(x_i - \hat{x}_i)/T_p = l + \rho$, where l is an integer, $|\rho| < 1$ and $\hat{x}_i$ is the receiver estimate of x_i. When $l = 0$, the PRN code phase of the received signal is acquired (which is represented by an H_1 state); otherwise, when $l \neq 0$, the receiver local PRN code is out of step with the received PRN code (which is represented by an H_0 state). Let y_k represent the correlation between the input PRN code and the receiver local PRN code over the kth correlation interval, i.e.,

$$y_k = \frac{1}{N}\sum_{i=(k-1)N}^{kN-1} P[(1+\zeta)iT_s - \xi T_p]\cdot P[(1+\hat{\zeta})iT_s - \hat{\xi}T_p] = \bar{y}_k + y_k^r \quad (5)$$

where $\bar{y}_k$ and y_k^r are the mean and random component of y_k, respectively. It can be derived that (see Appendix A)

$$\bar{y} = E[y_k] \approx R_I(\rho) \triangleq \begin{cases} (1-|\rho|), & H_1 \text{ state} \\ 0, & H_0 \text{ state} \end{cases} \quad (6)$$

where $R_I(\cdot)$ is an ideal two-level autocorrelation function of PRN codes, and

$$\mathrm{var}[y_k] = \mathrm{var}[y_k^r] \approx G(\rho) \triangleq \begin{cases} |\rho|^2/M, & H_1 \text{ state} \\ (1-2|\rho|+2|\rho|^2)/M, & H_0 \text{ state} \end{cases} \quad (7)$$

$\mathrm{var}[x]$ represents the variance of x, and $M = \mathrm{Int}(N\cdot Ts/Tp)$ is the integer code chip number over the correlation interval. Assuming that the parameters ζ, ξ, and ω_d are constant (although unknown) over the kth correlation interval, the outputs of the Average & Dump filters of the I and Q channels, at the end of the interval, can be obtained as

$$\begin{aligned} e_I(k) &\approx \tfrac{1}{2}AR_I[\rho(k)]\mathrm{sinc}\{[\Delta\omega_d(k)]N/2\}\cos\phi_k + \hat{n}_I(k) \\ e_Q(k) &\approx \tfrac{1}{2}AR_I[\rho(k)]\mathrm{sinc}\{[\Delta\omega_d(k)]N/2\}\sin\phi_k + \hat{n}_Q(k) \end{aligned} \quad (8)$$

where $\mathrm{sinc}(z) \triangleq \sin z/z$, $\phi_k = (\Delta\omega_d(k))\cdot(N-1)/2 + \phi_{k-1}$, $\Delta\omega_d(k) = \omega_d(k) - \hat{\omega}_d(k)$, $\hat{n}_I(k)$ and $\hat{n}_Q(k)$ are noise component due to the input noise $n(i)$,

$$\begin{aligned} \hat{n}_I(k) &= \frac{1}{N}\sum_{i=(k-1)N}^{kN-1} n(i)P[(1+\hat{\zeta})iT_s - \hat{\xi}T_p] \\ &\quad\times\cos[(\omega_b+\hat{\omega}_d(k))i] \\ &\quad+\tfrac{1}{2}Ay_k^r\,\mathrm{sinc}[\Delta\omega_d(k)N/2]\cos\phi_k \\ \hat{n}_Q(k) &= \frac{1}{N}\sum_{i=(k-1)N}^{kN-1} n(i)P[(1+\hat{\zeta})iT_s - \hat{\xi}T_p] \\ &\quad\times\sin[(\omega_b+\hat{\omega}_d(k))i] \\ &\quad+\tfrac{1}{2}Ay_k^r\,\mathrm{sinc}[\Delta\omega_d(k)N/2]\sin\phi_k. \end{aligned} \quad (9)$$

$e_I(k)$ and $e_Q(k)$ are approximately independent Gaussian random variables, their mean and variance are [11]

$$\begin{aligned} E[e_I(k)] &= D_k\cos\phi_k \\ E[e_Q(k)] &= D_k\sin\phi_k \\ \mathrm{var}[e_I(k)] &= \mathrm{var}[e_Q(k)] \\ &= \sigma_n^2/2N + \frac{A^2}{8}\left(\frac{T_s}{T_p}\right)^2 G[\rho(k)] \\ &\quad\times\mathrm{sinc}^2[(\Delta\omega_d(k))N/2] \end{aligned} \quad (10)$$

where $D_k = 0.5AR_I[\rho(k)]\mathrm{sinc}[(\Delta\omega_d(k))N/2]$, and σ_n is the variance of the input noise $n(i)$. From (10), the mean of $e_I(k)$ and $e_Q(k)$ increases as the code phase error $\rho(k)$ decreases and/or as the Doppler shift estimation error $\Delta\omega_d(k)$ decreases; and the variance of $e_I(k)$ and $e_Q(k)$ results from the input noise and from the estimation errors of the code phase and Doppler

shift. According to (6), within a full period of PRN codes only one correlation peak occurs at $\rho(k) = 0$, which allows unambiguous delay determination up to a maximum propagation delay equal to the period of code sequences (which is 1 ms for the C/A code). The input signal of the digital energy detector (as shown in Fig. 1) is

$$S^2(k) = e_I^2(k) + e_Q^2(k). \tag{11}$$

If the threshold of the detector is set to D_t^2, then an H_1 state is detected if the input of the energy detector $S^2(k)$ is larger than or equal to D_t^2, and an H_0 state is sensed if $S^2(k)$ is less than D_t^2. From the statistics of $e_I(k)$ and $e_Q(k)$, and (10), the detection and false-alarm probabilities of the PRN code phase acquisition, at the end of the kth correlation interval, can be obtained as follows (see Appendix B)

$$P_D(k) = \int_{\beta_k}^{\infty} \chi \cdot \exp[-\tfrac{1}{2}(\chi^2 + \gamma_k^2)] \cdot I_0(\gamma_k \chi) \cdot d\chi \tag{12}$$

$$P_{FA}(k) = \exp\left\{ -\frac{1}{2} \frac{D_n}{1 + \alpha\left(\frac{T_s}{T_p}\right)(1 - 2|\rho(k)| + 2|\rho(k)|^2)\mathrm{sinc}^2[(\Delta\omega_d(k))N/2]} \right\} \tag{13}$$

where

$$\gamma_k = \sqrt{2\alpha \cdot \frac{N(1 - |\rho(k)|)^2 \mathrm{sinc}^2[(\Delta\omega_d(k))N/2]}{1 + \alpha\left(\frac{T_s}{T_p}\right)|\rho(k)|^2 \mathrm{sinc}^2[(\Delta\omega_d(k))N/2]}} \tag{14}$$

$$\beta_k = \sqrt{\frac{D_n}{1 + \alpha\left(\frac{T_s}{T_p}\right)|\rho(k)|^2 \mathrm{sinc}^2[(\Delta\omega_{dk})N/2]}} \tag{15}$$

$I_0(\cdot)$ is zero-order modified Bessel function, $\alpha = (A/2)^2/\sigma_n^2 = (C/N_0)/B_{IF}$ is the signal-to-noise ratio of the spread spectrum input signal (B_{IF} is the receiver 3 dB IF bandwidth for the input PRN code signal), and $D_n = D_t^2 \cdot (N_0/4N)^{-1}$ is the normalized threshold. Fig. 2 shows the detection probability P_D and the false-alarm probability P_{FA} as functions of D_n, (C/N_0), $|\rho|$, $(\Delta\omega_d)N/2\pi$ and $NT_s(=T_n)$ for the C/A code channel with $B_{IF} = 2R_0$, based on (12)–(15). From Fig. 2, we can see that: 1) the detection probability P_D increases with the increase of the (C/N_0) value of the input signal and the correlation interval, and with the decrease of the Doppler shift estimation error, code phase estimation error and the normalized threshold of the energy detector; 2) the false-alarm probability P_{FA} decreases with the increase of the normalized threshold D_n; and 3) P_{FA} is, to a great extent, independent of the values of (C/N_0) which is between 35 dB-Hz and 45 dB-Hz, the Doppler shift estimation error, the code phase tracking error, and the correlation interval.

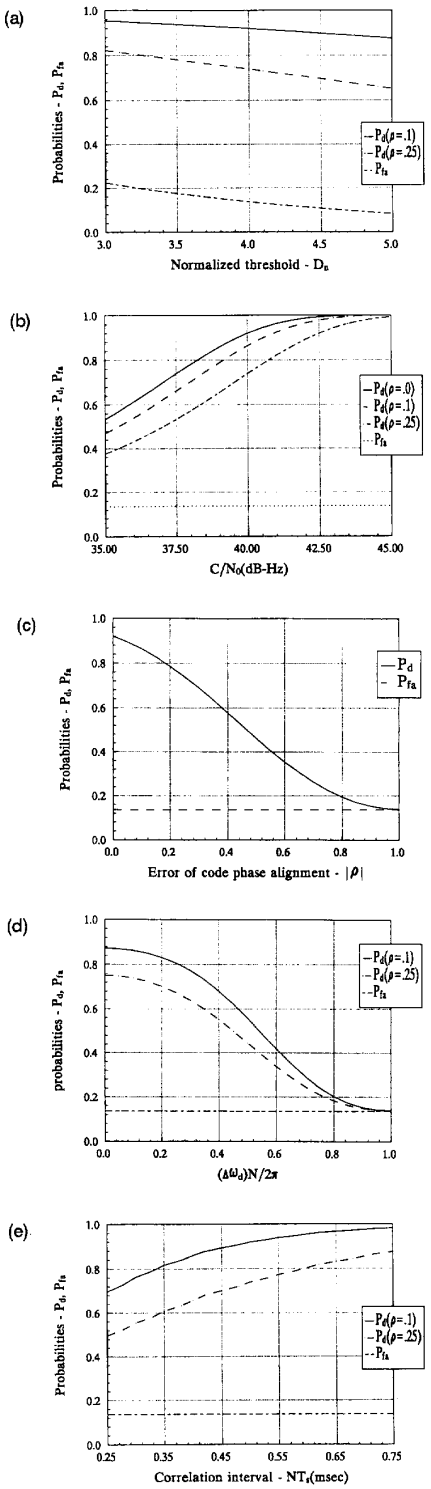

Fig. 2. Probabilities of detection and false-alarm for single-dwell search. (a) $C/N_0 = 40$ dB-Hz, $(\Delta\omega_d)N/2 = 0.1\pi$, $N = 1076$. (b) $(\Delta\omega_d)N/2 = 0.1\pi$, $D_n = 4.0$, $N = 1076$. (c) $C/N_0 = 40$ dB-Hz, $(\Delta\omega_d)N/2 = 0.1\pi$, $D_n = 4.0$. (d) $C/N_0 = 40$ dB-Hz, $D_n = 4.0$, $N = 1076$. (e) $C/N_0 = 40$ dB-Hz, $(\Delta\omega_d)N/2 = 0.1\pi$, $D_n = 4.0$, $N = 1076$.

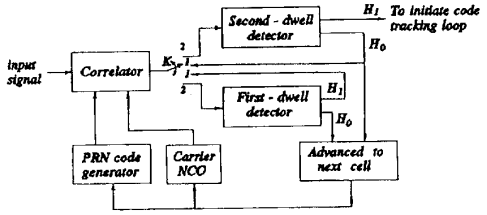

Fig. 3. Double-dwell search strategy.

Since $\alpha \ll 1$ corresponding to the (C/N_0) values, $P_{FA}(k) \approx \exp(-D_n/2)$, i.e., P_{FA} depends only on D_n.

From the performance analysis of the single-dwell search discussed above, the improvement of acquisition performance is limited by the following 3 factors. 1) Because of the Doppler shift uncertainty $\Delta\omega_d(k) \neq 0$, the detector performance is deteriorated by a factor of $\text{sinc}^2[(\Delta\omega_d(k))N/2]$, which restricts the increase of the dwell (correlation) interval, i.e., the value of N. 2) The increase of the despreading gain is limited because of the limit on increasing N. 3) With a low input (C/N_0) value, in order to reduce P_{FA}, D_n should be increased, which also reduces P_D. The high P_{FA} (as shown in Fig. 2) results in a very large value of the average acquisition time. Consequently, a double-dwell search strategy is necessary to improve the acquisition performance (i.e., to reduce the average acquisition time) [4–5], as shown in Fig. 3. In the first dwell detection with immediate rejection, the small dwell interval results in a fast search through the uncertainty regions, a low threshold prevents P_D from being too low and increases P_{FA} (which is reduced in the second dwell). If an H_0 state is detected in the first dwell, the correlation is continued with the local code phase delay and carrier frequency of the next reference cell; otherwise, if a tentative H_1 state is assumed in the first dwell, a second dwell (verification mode) starts. The second dwell uses the same detector as that of the first dwell, but sequentially performs several tests after which a majority decision is made. If at least B of A tests indicate coarse synchronization, then an H_1 state is verified and the code tracking loop is activated; otherwise, the synchronization control scheme updates the local code phase and the cell-by-cell testing format is continued. The short correlation interval restricts the detector performance deterioration due to the uncertainty of the Doppler shift. The input code signal and the locally generated code signal are correlated and their phase alignment is detected in one segment (or the average interval) uncorrelated with other segments because of the "dump" operation in the Average & Dump filters. The input noises of different segments are independent of each other and the possible weak correlation among the PRN codes of each segment is negligible while taking the low (C/N_0) value of the input signal into account. The correlation and detection of different segments are therefore independent of each other. Let P_{D1} and P_{FA1} represent the detection and false-alarm probabilities, respectively, for the first-dwell search, P_{D2} and P_{FA2} for the second-dwell search, then with the independent tests the probabilities of the double-dwell search on each reference cell are [12]

$$P_D = P_{D1}P_{D2} = \sum_{n=B}^{A} \binom{A}{n} P_{D1}^{n+1}(1-P_{D1})^{A-n}$$
$$P_{FA} = P_{FA1}P_{FA2} = \sum_{n=B}^{A} \binom{A}{n} P_{FA1}^{n+1}(1-P_{FA1})^{A-n}. \quad (16)$$

Fig. 4 shows the probabilities P_D and P_{FA} of the double-dwell system as a function of (C/N_0) for the C/A code channel. Comparing Fig. 4 with Fig. 2(b), we can observe that the double-dwell search strategies dramatically reduce P_{FA}, but only slightly reduce P_D when the value of (C/N_0) is relatively large. As a result, the average acquisition time can be significantly reduced, which means that the acquisition performance is greatly improved.

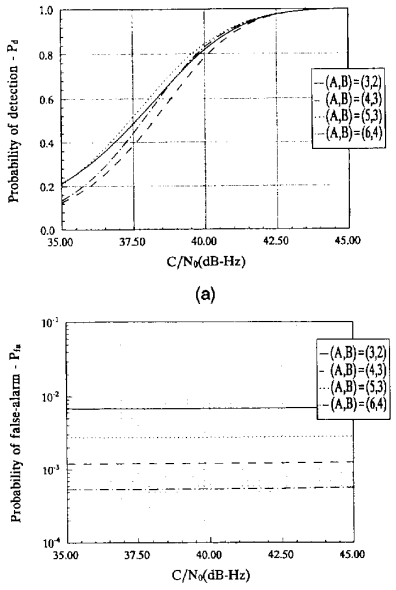

Fig. 4. (a) Detection probability for double-dwell search: $(\Delta\omega_d)N/2 = 0.1\pi$, $D_n = 4.0$, $N = 1076$, $\rho = 0.1$. (b) False-alarm probability for double-dwell search: $(\Delta\omega_d)N/2 = 0.1\pi$, $D_n = 4.0$, $N = 1076$, $\rho = 0.1$.

III. CODE PHASE TRACKING

Accurate synchronization between the input and local PRN code signals is accomplished by a DDLL as shown in Fig. 5. With the initial delay error less than the loop pull-in range, the loop provides the MLE of the time delay in the presence of Gaussian noise [6–7]. A practical implementation of the loop makes use of correlation operations between the input

signal and two different phase delayed (early and late) local PRN codes [9]. The code tracking loop to be modeled here is a noncoherent, early-late, DDLL, with two independent correlators for discriminating code phase error. The DDLL design goal is to achieve low root-mean-square (rms) tracking jitter in the presence of input white Gaussian noise while tracking the input PRN code phase dynamics due to the relative motion between the satellite and the receiver. The overall variance σ_ρ^2 of the code tracking error is used as the loop performance criterion.

Noncoherent Early–Late DDLL Modeling: Let "+" sign represent the early (E) correlator and "−" sign the late (L) correlator, and δ represent 1/2 code phase offset normalized to code chip width T_p between the local PRN code generators for the early and late correlators, respectively, then the in-phase and quadrature signals of the local signal generator, at the ith sample, are

$$\begin{aligned} I_{I\pm}(i) &= P[(1+\hat{\zeta})iT_s - \hat{\xi}T_p \pm \delta T_p] \cdot \cos[(\omega_b + \hat{\omega}_d)i] \\ I_{Q\pm}(i) &= P[(1+\hat{\zeta})iT_s - \hat{\xi}T_p \pm \delta T_p] \cdot \sin[(\omega_b + \hat{\omega}_d)i]. \end{aligned} \tag{17}$$

If we define

$$\begin{aligned} K_0 &= \frac{A^2}{4}\operatorname{sinc}^2[(\Delta\omega_d)N/2], \\ D_\Delta(\rho,\delta) &= R^2(x)|_{x=\rho-\delta} - R^2(x)|_{x=\rho+\delta} \end{aligned} \tag{18}$$

where

$$R(x) \triangleq \overline{P[(1+\zeta)iT_s + \tau_0] \cdot P[(1+\hat{\zeta})iT_s + \tau_0 + xT_p]}$$

(with the average operation being performed over time variable i, τ_0 being an arbitrary code phase shift) approximates to the autocorrelation function of the PRN code with normalized code phase error x, then it can be derived that the output of the code phase discriminator (Fig. 5) as a function of ρ and δ, at the end of the kth correlation interval, is [11]

$$\begin{aligned} D(k,\rho,\delta) &= L(k,\rho,\delta) - E(k,\rho,\delta) \\ &\triangleq K_0 D_\Delta(\rho,\delta) + N_D(k,\rho,\delta) \end{aligned} \tag{19}$$

where $L(k,\rho,\delta)$ and $E(k,\rho,\delta)$ are the output of the late and early channel correlators, $N_D(k,\rho,\delta)$ is

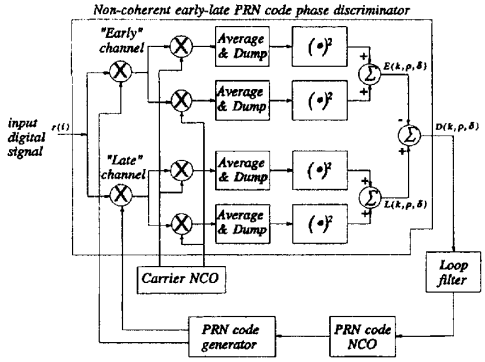

Fig. 5. Noncoherent full-time early-late DDLL.

the equivalent noise component. For the C/A code which is Gold code with period of 1023 chips, the autocorrelation function is $R(x) = R_I(x) + n_R(x)$, where $n_R(x)$ is an equivalent noise component of $R(x)$,

$$n_R(x) = \begin{cases} -1/1023, & p = 0.75 \\ -65/1023, & p = 0.125 \\ +63/1023, & p = 0.125 \end{cases} \tag{20}$$

(p stands for probability). The error component of $D_\Delta(\rho,\delta)$ due to $n_R(x)$ is

$$\begin{aligned} N_R(\rho,\delta) &= [R^2(x)|_{x=\rho-\delta} - R^2(x)|_{x=\rho+\delta}] \\ &\quad - [R_I^2(x)|_{x=\rho-\delta} - R_I^2(x)|_{x=\rho+\delta}] \\ &= 2n_R(x)|_{x=\rho-\delta} \cdot R_I(x)|_{x=\rho-\delta} + n_R^2(x)|_{x=\rho-\delta} \\ &\quad - 2n_R(x)|_{x=\rho+\delta} \cdot R_I(x)|_{x=\rho+\delta} - n_R^2(x)|_{x=\rho+\delta}. \end{aligned} \tag{21}$$

When $|\rho| \to 0$, $(\rho-\delta)$ and $(\rho+\delta)$ are related to different chip durations, so that $n_R(x)|_{x=\rho-\delta}$ and $n_R(x)|_{x=\rho+\delta}$ are uncorrelated with $E\{N_R(\rho,\delta)\} = -4\rho/1023 \approx 0$, $E\{N_R^2(\rho,\delta)\} \approx 8\cdot[1+(\delta-\rho)^2]/1023 \approx 8\cdot(1+\delta^2)/1023$, the effect of $N_R(\rho,\delta)$ may be neglected. For P code phase tracking, because of the very long code period, the autocorrelation function may be taken as $R_I(x)|_{x=\rho+\delta}$ and $R_I(x)|_{x=\rho-\delta}$ for the early and late correlators, respectively, with very little error when the sample number N of each correlation interval is much larger than one [13]. Substituting $R_I(\cdot)$ defined in (6) into (18), we obtain

$$D_\Delta(\rho,\delta) = \begin{cases} \left.\begin{array}{ll} 1+(\rho-\delta)(\rho-\delta-2), & 1-\delta \le \rho \le 1+\delta \\ 4\delta(1-\rho), & \delta \le \rho \le 1-\delta \\ 4\rho(1-\delta), & 0 \le \rho \le \delta \end{array}\right\} & \text{if } 0 \le \delta \le \frac{1}{2} \\ \left.\begin{array}{ll} 1+(\rho-\delta)(\rho-\delta-2), & \delta \le \rho \le 1+\delta \\ 1+(\rho-\delta)(\rho-\delta+2), & 1-\delta \le \rho \le \delta \\ 4\rho(1-\delta), & 0 \le \rho \le 1-\delta \end{array}\right\} & \text{if } \frac{1}{2} \le \delta \le 1 \\ 0, & \rho \ge 1+\delta \end{cases} \tag{22}$$

for $\rho \geq 0$, and $D_\Delta(+\rho,\delta) = -D_\Delta(-\rho,\delta)$ for $\rho \leq 0$. Plotting $D_\Delta(\rho,\delta)$ versus ρ (with a constant δ) we can obtain the so-called discriminator S-curves for the noncoherent early–late DDLL as in the analog delay lock loop [8]. It has been shown [11] that the total output noise $N_D(k,\rho,\delta)$ of the discriminator is still white noise (due to the "dump" operations in the Average & Dump low-pass (LP) filters) with equivalent one-side power spectral density

$$N_L = 2\left(\frac{N_0}{2}\right)^2 B_L[1 - R^2(2\delta)] + \frac{A^2}{4}\left[\frac{1}{2}\left(\frac{N_0}{2}\right)\right]\operatorname{sinc}^2[(\Delta\omega_d)N/2]f(\rho,\delta) \tag{23}$$

where

$$f(\rho,\delta) = R^2(\rho-\delta) + R^2(\rho+\delta) - 2R(\rho-\delta)R(\rho+\delta)R(2\delta) \tag{24}$$

and $B_L(=\pi/N)$ is the equivalent bandwidth of the LP filters. The power spectral density N_L gives no information about the probability density function of this output noise. Although the input noise is Gaussian, the nonlinear transformation (such as the square function) assures that the output statistics are non-Gaussian. However, when the tracking error $\rho(k)$ is very small, the code phase discriminator is operating in its linear region and the discriminator output random process $N_D(k,\rho,\delta)$ is Gaussian.

DDLL Tracking Performance in the Absence of Noise: It can be seen from (22) that for $0 \leq \delta \leq \frac{1}{2}$, $D_\Delta(\rho,\delta)$ is a linear function of ρ with slope $D'_\Delta(\rho,\delta) = 4(1-\delta)$ when $|\rho| \leq \delta$. Therefore, in the case of small code phase tracking error, the phase discriminator can be modeled by a linear function, $D_\Delta(\rho,\delta) = S_0(\delta)\cdot\rho$, where $S_0(\delta) = 4(1-\delta)$ is the slope of $D_\Delta(\rho,\delta)$. From (19), we have

$$D(k,\rho,\delta) = K_0 D_\Delta(\rho,\delta) + N_D(k,\rho,\delta) = K(\delta)\cdot\rho + N_D(k,\rho,\delta) \tag{25}$$

where $K(\delta) = K_0 \cdot S_0(\delta) = A^2\cdot(1-\delta)\cdot \operatorname{sinc}^2[(\Delta\omega_d)N/2]$. Let $z\{\cdot\}$ be the unit delay operator $z\{x(k)\} = x(k+1)$ and $z^{-1}\{x(k)\} = x(k-1)$, then with the transfer function of the loop filter $F(z)$, and the transfer function of the PRN code NCO $D(z)$ $(= z^{-1}/(1-z^{-}))$, the normalized phase delay estimate $\hat{\xi}$ of local PRN code can be obtained based on the output of the code phase discriminator $D(k,\rho,\delta)$,

$$\hat{\xi}(k) = D(z)F(z)D(k,\rho,\delta). \tag{26}$$

The functionally equivalent mathematical model of the DDLL is shown in Fig. 6. Substituting (25) and

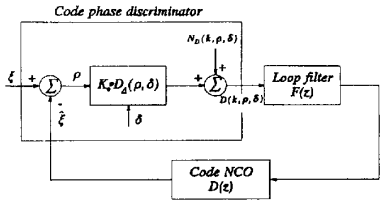

Fig. 6. Mathematical model of DDL.

$\rho = \xi - \hat{\xi}$ into (26),

$$\hat{\xi}(k) = D(z)F(z)\{K(\delta)[\xi(k) - \hat{\xi}(k)] + N_D(k,\rho,\delta\} = K(\delta)D(z)F(z)\left\{[\xi(k) - \hat{\xi}(k)] + \frac{N_D(k,\rho,\delta)}{K(\delta)}\right\}. \tag{27}$$

If we define the loop transfer function for the input code phase and the equivalent noise as

$$H_\xi(z) = \frac{z-1}{K(\delta)F(z) + (z-1)}, \qquad H_N(z) = \frac{K(\delta)F(z)}{K(\delta)F(z) + (z-1)} \tag{28}$$

respectively, then from (27) we can obtain

$$\rho(k) = H_\xi(z)\xi(k) - H_N(z)\frac{N_D(k,\rho,\delta)}{K(\delta)}. \tag{29}$$

It is obvious from (29) that the tracking error $\rho(k)$ consists of two components, one due to the system dynamics represented by the first term and the other due to input noise represented by the second term.

Because of the relative movement between the satellite and receiver, the input code phase varies with time. The DDLL must be able to track the variations and to maintain the tracking errors within an allowable limit. According to (28)–(29), the loop tracking error due to $\xi(k)$ is

$$\rho(k) = \frac{z-1}{K(\delta)F(z) + (z-1)}\xi(k). \tag{30}$$

A stable 1st-order loop (with $F(z) = g_1$, and loop gain $G_1 = K(\delta)\cdot g_1$) can track a phase step input $\xi(k) = a\cdot U(k)$ with steady tracking error $\rho(\infty) = 0$, a frequency step input signal $\xi(k) = a\cdot k\cdot U(k)$ with $\rho(\infty) = a/G_1$. For a 2nd-order loop, $F(z) = g_1 + g_2/(1-z^{-1})$, loop gain parameters are $G_1 = K(\delta)\cdot g_1$, $G_2 = K(\delta)\cdot g_2$. A stable 2nd-order loop can track a phase step input and a frequency step input with $\rho(\infty) = 0$, and a frequency ramp input $\xi(k) = a\cdot k^2\cdot U(k)$ with $\rho(\infty) = 2a/G_2$. Transient responses of 1st- and 2nd-order linear DDLLs can be obtained by solving (30). The z-transform of the unit-impulse response is often referred to as the system function. A necessary and sufficient condition of system stability is that the poles of the system function must lie inside the unit circle

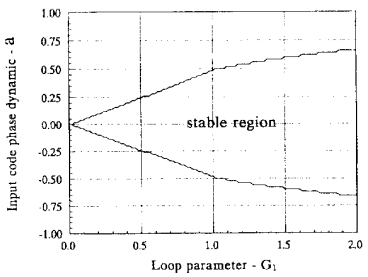

Fig. 7. Stable region of 1st-order nonlinear DDLLs: frequency-step input ($\rho(0) = 0.0$).

of the z-plane [14], therefore, the stable range of loop gain is $0 < G_1 < 2$ for a 1st-order loop, $r > 1$ and $0 < G_1 < 4/(r+1)$ for a 2nd-order loop where $r \triangleq 1 + (G_1/G_2)$.

With the decrease of the input (C/N_0) ratio, the code phase delay tracking error $\rho(k)$ increases, which may exceed the linear region of the discriminator characteristic $D_\Delta(\rho,\delta)$. As a result, a nonlinear theory should be used to analyze the loop performance in the situations of a low (C/N_0) ratio. In this case the condition of loop stability is stricter than in the case of linear code phase discriminator. The loop stability depends on loop filter gain(s), initial tracking error(s) and input code phase delay dynamics.

1) *1st-order loop*: With $N_D(k,\rho,\delta) = 0$, from (28)–(29), the tracking error iterative equation is

$$\rho(k+1) - \rho(k) = [\xi(k+1) - \xi(k)] - G_1 D_\Delta[\rho(k),\delta]. \tag{31}$$

The variation of code phase tracking error $\rho(k+1) - \rho(k)$ is the difference between the dynamics of the input code phase represented by $\xi(k+1) - \xi(k)$ and the dynamics tracking ability of the loop represented by $G_1 \cdot D_\Delta[\rho(k),\delta]$ (with the loop gain of G_1). The transient responses can be obtained by recursively solving (31) with defined input code phase dynamics $\xi(k+1) - \xi(k)$. It is shown that the transient response durations are shorter when the loop gain G_1 is closer to 1.0. According to the recursive analysis of (31), the loop can track a step phase input with steady-state tracking errors $\rho_{ss} = 0$ if the initial tracking error $|\rho(0)| < 1 + \delta$ and the loop filter gain $0 < G_1 < 2$. An example of two-dimensional parameter ranges for loop stability with a frequency step input is shown in Fig. 7. With low input code phase dynamics (small $|a|$ value), the loop can track the phase dynamics, which results in small code phase tracking errors and the code phase discriminator stays in the linear region. Hence, the loop stable region for the dynamics $|a|$ increases almost linearly with the increase of the loop gain G_1. On the other hand, with high dynamics of the input code phase (large $|a|$ value), the loop has a large tracking error and the phase discriminator stays in the nonlinear region. Consequently, the stable region for the dynamics $|a|$ does not increase linearly with the increase of the loop gain G_1. It is clear that the DDLL stable region is becoming smaller with the increase of the input code phase dynamics.

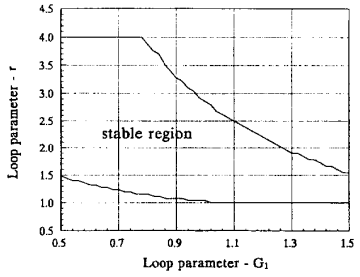

(a)

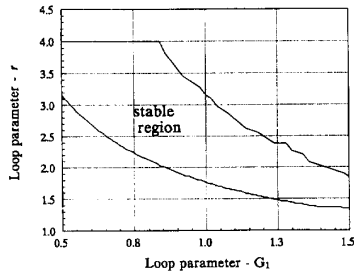

(b)

Fig. 8. Stable region of 2nd-order nonlinear DDLLs. (a) Frequency-step input ($a = 0.5$, $\rho(-1) = 0.0$, $\rho(0) = 0.0$). (b) Frequency-ramp input ($a = 0.25$, $\rho(-1) = 0.0$, $\rho(0) = 0.0$).

2) *2nd-order loop*: The code tracking error iterative equation of a 2nd-order loop is

$$\begin{aligned}\rho(k+2) - 2\rho(k+1) + \rho(k) &= [\xi(k+2) - 2\xi(k+1) + \xi(k)] - (G_1 + G_2) \\ &\quad \cdot D_\Delta[\rho(k+1),\delta] + G_1 \cdot D_\Delta[\rho(k),\delta].\end{aligned} \tag{32}$$

The transient responses of the loop to input code phase $\xi(k)$ can be obtained by recursively solving (32). It is observed that a 2nd-order stable loop can track a frequency step input signal with steady-state tracking error $\rho_{ss} = 0$ and a frequency ramp input signal with steady-state tracking error $\rho_{ss} = 2a/G_2$. Examples of the loop stable regions are shown in Fig. 8. In Fig. 8(a), when G_1 is small (say, $G_1 < 0.8$), the stable region for r value is reduced compared with that of a linear loop; when G_1 is large, the phase discriminator works in the linear region, so that the stable region is close to that of a linear loop. In Fig. 8(b), the input code phase is changed from the lower dynamic waveform (frequency-step, Fig. 8(a)) to the higher

dynamic waveform (frequency-ramp), therefore, the stable region is reduced when compared with that of Fig. 8(a). The low bound value for r should be larger than that of Fig. 8(a) in order to track the frequency-ramp input.

From the above analysis, we can conclude the following. 1) While the code phase discriminator works in both linear and nonlinear regions, the region of stable loop gain(s) is smaller in the nonlinear case. 2) For stable loops, the steady-state tracking error is independent of the nonlinear characteristics of the discriminator, since the stable loop operates in the linear region of the discriminator characteristic curve at steady-state irrespective of the initial tracking error. 3) Concerning the transient response, the optimum loop gain(s) is $G_1 = 1.0$ for the 1st-order loop and $G_1 = 1.0$, $r = 2.0$ for the 2nd-order loop. 4) As δ increases, the loop hold-in range increases, however, the loop equivalent gain(s) decreases according to (25), which may increase the tracking error and transient duration. Therefore, larger δ should be chosen to increase the loop hold-in range with lower (C/N_0) values, and smaller δ should be chosen to enhance loop dynamic capability with higher system dynamics. 5) When the system dynamic (represented by the value of $|a|$ in the input code phase) increases to an appropriate high value, the 1st-order loop with a frequency-step input code phase and the 2nd-order loop with a frequency-ramp input code phase are not stable no matter what the loop gain(s) and initial tracking error(s) are. The 1st-order loop can track the input PRN code phase with the relative velocity component (between the satellite and the receiver in the direction of the pseudo-range) up to $|a|_{\max} \cdot c \cdot f_s/(N \cdot R)$, where $|a|_{\max}$ is the maximum $|a|$ for the stable loop, c is the velocity of the electromagnetic wave. The 2nd-order loop can track the input PRN code phase delay with the acceleration of the relative movement (between the satellite and the receiver in the direction of the pseudo-range) up to $|a|_{\max} \cdot c \cdot f_s/(N \cdot R)$. Therefore, the correlation interval N (which is inversely proportional to the loop predetection bandwidth B_L) plays a very important role in the loop dynamic performance. Smaller N values should be used in cases of higher system dynamics.

DDLL Tracking Performance in the Presence of Noise: Here, we consider the linear analysis of the code phase tracking error due to input noise. With the input stationary zero-mean Gaussian noise $n(i)$, $N_D(k,\rho,\delta)$ is stationary with zero mean and wide band because of the narrow closed-loop bandwidth. As a result, the steady-state variance of $\rho(k)$ due to the approximated white noise $N_D(k,\rho,\delta)$ is given by [14]

$$\sigma_\rho^2 = \frac{1}{2\pi j}\oint_{|z|=1} H_N(z)H_N(z^{-1})z^{-1}R_N(z)\,dz \quad (33)$$

where $R_N(z)$ is the z-transform of the autocorrelation function $R_{ND}(k)$ of $N_D(k,\rho,\delta)$ normalized to $K^2(\delta)$, i.e., $R_N(z) = z\{R_{ND}(k)/K^2(\delta)\} = N_L B_L/K^2(\delta)$, so that

$$\sigma_\rho^2 = \frac{N_L B_L}{K^2(\delta)}\frac{1}{2\pi j}\oint_{|z|=1} H_N(z)H_N(z^{-1})z^{-1}\,dz = \frac{N_L B_{cl}}{K^2(\delta)} \quad (34)$$

with

$$B_{cl} \triangleq B_L \cdot \frac{1}{2\pi j}\oint_{|z|=1} H_N(z)H_N(z^{-1})z^{-1}\,dz \quad (35)$$

being defined as the one-sided closed-loop bandwidth. As noticed in (19) and (23)–(24), $N_D(k,\rho,\delta)$ is a function of ρ. In order to pursue linear theory it is assumed that $N_D(k,\rho,\delta)$ is independent of ρ for small ρ. We define $N_D(k,\delta) \triangleq N_D(k,\rho,\delta)|_{\rho=0}$ since in the linear region $\rho(k)$ is very small with a relatively high input (C/N_0) ratio, then from (23),

$$N_L \approx N_L|_{\rho=0} = 2\left(\frac{N_0}{2}\right)^2 B_L[1 - R^2(2\delta)] + \frac{A^2}{4}\left(\frac{N_0}{2}\right)\mathrm{sinc}^2[(\Delta\omega_d)N/2](1-\delta)^2[1 - R(2\delta)]. \quad (36)$$

Substituting (36) into (34),

$$\sigma_\rho^2 = \frac{1}{2\alpha_{cl}}\left\{\frac{1 - R^2(2\delta)}{\alpha_L(1-\delta)^2\mathrm{sinc}^4[(\Delta\omega_d)N/2]} + \frac{1 - R(2\delta)}{4\mathrm{sinc}^2[(\Delta\omega_d)N/2]}\right\} \quad (37)$$

where $\alpha_{cl} = A^2/(N_0 \cdot B_{cl})$ is the SNR in the closed-loop bandwidth B_{cl}, and $\alpha_L = A^2/(N_0 \cdot B_L)$ is the SNR in the Average & Dump LP filter output. Let us define

$$S_L = \frac{4(1-\delta)^2\mathrm{sinc}^4[(\Delta\omega_d)N/2]}{[1 - R(2\delta)]\{4\alpha_L^{-1}[1 + R(2\delta)] + (1-\delta)^2\mathrm{sinc}^2[(\Delta\omega_d)N/2]\}} \quad (38)$$

as the "square loss" of the DDLL (corresponding to that defined in [8] for an analog delay lock loop) which is a function of δ, α_L, N, and $(\Delta\omega_d)$, then

$$\sigma_\rho^2 \triangleq \frac{1}{2\alpha_{cl}S_L}. \quad (39)$$

From (38)–(39), we observe the following. 1) S_L would increase as a result of a) a decrease of the Doppler estimation error $(\Delta\omega_d)$, or b) an increase of the sampling number N in each correlation interval if $(\Delta\omega_d) = 0$, or c) an increase of the SNR of the Average & Dump LP filter output. 2) If $(\Delta\omega_d) \neq 0$, both N and $\mathrm{sinc}[(\Delta\omega_d)N/2]$ affect S_L, depending on

the value of $(\Delta\omega_d)$. 3) σ_ρ^2 decreases with either an increase of loop SNR ratio α_{cl} or an increase of the "square loss" S_L. 4) The loop SNR α_{cl} increases as B_{cl} decreases, which is a function of the loop filter $F(z)$ and is inversely proportional to N. For a 1st-order loop,

$$H_N(z) = \frac{G_1}{z + (G_1 - 1)}, \qquad B_{cl} = \frac{G_1}{2 - G_1} \cdot B_L \tag{40}$$

and for a 2nd-order loop,

$$H_N(z) = \frac{(G_1 + G_2)z - G_1}{z^2 + [(G_1 + G_2) - 2]z + [1 - G_1]}, \qquad B_{cl} = \frac{2G_2 + G_1G_2 + 2G_1^2}{G_1[4 - G_2 - 2G_1]} \cdot B_L. \tag{41}$$

From (25), $K(\delta)$ is a function of the input signal power, the Doppler estimation error $(\Delta\omega_d)$, the correlation interval N and the discriminator parameter δ, so are the loop equivalent gains G_1 and G_2. The equivalent loop gain increases as the input signal power increases and as δ and/or $[(\Delta\omega_d)N/2]$ decreases. The analysis of the variance of the code phase tracking error has been verified by computer simulations, as shown in Fig. 9. Each value of the simulation results is obtained based on 30 s data (after the code phase acquisition) with sampling frequency f_s = 2.1518 MHz for the C/A code phase synchronization.

The performance tradeoff between tracking errors due to the system dynamics and those due to the input noise is of primary consideration when selecting loop parameters. From (40)–(41), loop gains G_1 and G_2 should be small in order to reduce the tracking error due to the input noise. On the other hand, loop gains G_1 and G_2 should be large in order to reduce the steady-state tracking error due to system dynamics. Another important parameter is the correlation interval N, which controls the equivalent bandwidth of the Average & Dump LP filter. In the case of low system dynamics, small G_1, G_2 and large N should be used to reduce the closed-loop bandwidth, so that the tracking error (mostly due to input noise) is suppressed. In the case of high system dynamics, large G_1, G_2 and small N should be used, so that the closed-loop bandwidth is large enough to track the dynamics of the input PRN code phase.

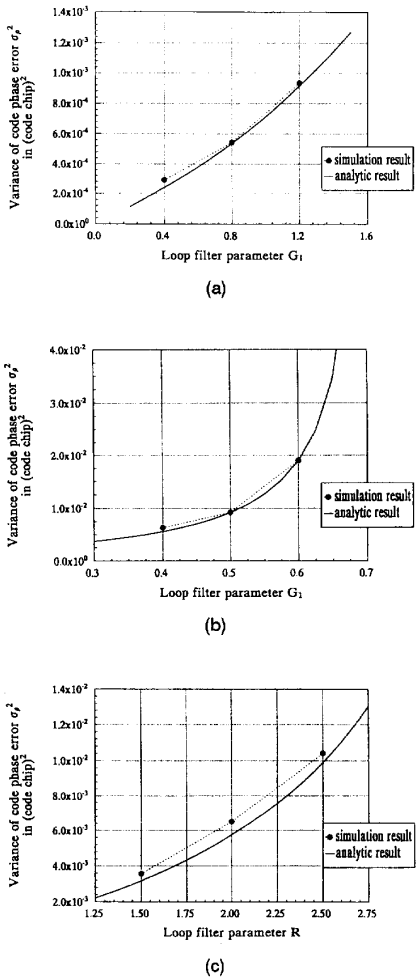

Fig. 9. Variances of code phase tracking error. (a) 1st-order DDLL: T_n = 20 ms, C/N_0 = 40 dB-Hz, $(\Delta\omega_d)N/2 = 0.1\pi$, δ = 0.5. (b) 2nd-order DDLL: T_n = 20 ms, C/N_0 = 40 dB-Hz, $(\Delta\omega_d)N/2 = 0.15\pi$, δ = 0.5, R = 2.0. (c) 2nd-order DDLL: T_n = 20 ms, C/N_0 = 40 dB-Hz, $(\Delta\omega_d)N/2 = 0.1\pi$, δ = 0.5, G_1 = 0.4.

IV. CONCLUSIONS

The digital PRN code acquisition and tracking systems in the GPS receiver for the GPS pseudo-range observable have been modeled and evaluated mathematically. According to the MLE theory, the noncoherent correlations between the input signals and the receiver locally generated signals are performed for the initial coarse estimate of the input PRN code phases and the Doppler frequency shifts. A digital energy detector is modeled to detect the completion of the acquisition process. The derived closed-form expressions of the detection and false-alarm probabilities show that, the probabilities depend on the PRN code phase alignment error, the (C/N_0) of the input signal, the carrier phase error caused by the Doppler shift estimation error, the normalized detector threshold and the length of the correlation interval. The double-dwell, straight line (for the L1-C/A channel) and expanding-window (for the L1-P and L2-P channels) serial-search strategies are used because of their advantages over the single-dwell strategies in the average acquisition time.

The full-time early-late DDLLs are then modeled and investigated to lock the code phases of the receiver locally generated PRN codes to the PRN code phases of the input GPS signals for a fine synchronization. On the basis of the power spectral density analysis of both input signal and noise, the closed-form expression of the variance of code phase tracking error due to input noise has been derived. Both linear and nonlinear DDLLs are analyzed. The effects of the loop structures and parameters on the accuracy of the pseudo-range observable are studied. The DDLLs with higher order and higher gain loop filters have smaller tracking errors and shorter transient response duration in response to high dynamics of the input code phase. On the other hand, the DDLLs with lower order and lower gain loop filters are more stable and have smaller tracking errors resulting from the input noise. Therefore, it is necessary to design the loops with various loop bandwidth according to the applications of various system dynamics in order to optimize the DDLL performance.

With the input code phase being accurately aligned, the GPS receiver may start coherent code phase tracking after the carrier phase is acquired and locked. Furthermore, a carrier-aiding technique may be used with the DDLLs to significantly reduce coherent code phase tracking errors [10].

APPENDIX A. MEAN AND VARIANCE OF THE PRN CODE CORRELATION

From (5),

$$\bar{y} = E\left\{\frac{1}{N}\sum_{n-0}^{N-1} P[(1+\zeta)nT_s - \xi T_p]P[(1+\hat{\zeta})nT_s - \hat{\xi}T_p]\right\}$$
$$\approx E\left\{\frac{1}{T_n}\int_0^{T_n} P[(1+\zeta)t - \xi T_p]P[(1+\hat{\zeta})t - \hat{\zeta}T_p]\,dt\right\}. \tag{42}$$

The code phase delay between the input PRN code and local PRN code is

$$\varepsilon = [(1+\zeta)nT_s - \xi T_p] - [(1+\hat{\zeta})nT_s - \hat{\xi}T_p] = lT_p + \rho T_p \tag{43}$$

where $|\rho| < 1$, $l = 0$ in an H_1 state and $l \neq 0$ in an H_0 state. Assume the local PRN code rate is very close to the input PRN code rate, then from [15–16],

$$P(x_i)P(x_i + lT_p + \rho T_p)$$
$$= \sum_{n=-\infty}^{\infty} P(nT_p)P[(n+l)T_p]q(x_i - nT_p)$$
$$+ \sum_{n=-\infty}^{\infty} P(nT_p)P[(n+l+1)T_p]h(x_i - nT_p) \tag{44}$$

where x_i is defined in (1) and

$$q(t) = \begin{cases} 1, & 0 \le t \le (1-|\rho|)T_p \\ 0, & \text{otherwise} \end{cases}$$
$$h(t) = \begin{cases} 1, & (1-|\rho|)T_p \le t \le T_p \\ 0, & \text{otherwise} \end{cases}. \tag{45}$$

Define the autocorrelation function of the PRN code as

$$R^M(i,l) \triangleq T_p \sum_{m=0}^{M-1} P[(i+m)T_p]P[(i+m+l)T_p] \tag{46}$$

with

$$E[R^M(i,l)] = \begin{cases} M, & \text{if } l = 0 \\ -1, & \text{if } l \neq 0 \end{cases}$$
$$E[R^M(i,l)]^2 = \begin{cases} M^2, & \text{if } l = 0 \\ M, & \text{if } l \neq 0 \end{cases} \tag{47}$$

where $M = \text{int}(N \cdot T_s/T_p)$, then

$$\bar{y} \approx E\left\{\frac{1}{T_n}\int_0^{T_n}\left[\sum_{j=-\infty}^{\infty} P(jT_p)P[(j+l)T_p]q(t - \hat{\xi}T_p - jT_p)\right.\right.$$
$$\left.\left. + \sum_{j=-\infty}^{\infty} P(jT_p)P[(j+l+1)T_p]h(t - \hat{\xi}T_p - jT_p)\right]dt\right\}$$
$$= E\left\{\frac{1}{M}\sum_{j=0}^{M-1} P(jT_p)P[(j+l)T_p]\left(\frac{1}{T_p}\right)\int_0^{T_p} q(t)\,dt\right.$$
$$\left. + \frac{1}{M}\sum_{j=0}^{M-1} P(jT_p)P[(j+l+1)T_p]\left(\frac{1}{T_p}\right)\int_0^{T_p} h(t)\,dt\right\}$$
$$= (1-|\rho|)E[R^M(0,l)] + |\rho|E[R^M(0,l+1)]. \tag{48}$$

For $N \gg 1$, in an H_1 state ($l = 0$),

$$\bar{y} = \{(1-|\rho|)E[R^M(0,0)] + |\rho|E[R^M(0,1)]\}/M$$
$$= (1-|\rho|) - |\rho|/M$$
$$\approx (1-|\rho|) \tag{49}$$

and in an H_0 state ($l \neq 0$),

$$\bar{y} = \{(1-|\rho|)E[R^M(0,l)] + |\rho|E[R^M(0,l+1)]\}/M \approx 0. \tag{50}$$

Combining (48) with (50), (6) is achieved. For the variance of y of (5),

$$\text{var}[y|H_i] = E[y|H_i]^2 - \{E[y|H_i]\}^2, \qquad i = 0,1 \tag{51}$$

where

$$E[y|H_1]^2 = \{(1-|\rho|)E[R^M(0,0)]^2 + |\rho|^2 E[R^M(0,1)]^2\}/M^2$$
$$= (1-|\rho|)^2 + |\rho|^2/M \quad (52)$$
$$E[y|H_0]^2 = \{(1-|\rho|)^2 E[R^M(0,l)]^2 + |\rho|^2 E[R^M(0,l+1)]^2\}/M^2$$
$$= (1-|\rho|)^2/M + |\rho|^2/M$$
$$= (1-2|\rho|+2|\rho|^2)/M. \quad (53)$$

Substituting (49)–(50) and (52)–(53) into (51), (7) is obtained.

APPENDIX B. DETECTION AND FALSE-ALARM PROBABILITIES

Since $e_I(k)$ and $e_Q(k)$ are approximately independent Gaussian random variables, from (10), the joint probability density function of $e_I(k)$ and $e_Q(k)$ is

$$p(e_I(k), e_Q(k)|\phi_k) = \frac{1}{2\pi\sigma^2}\exp\left\{-\frac{1}{2\sigma^2}[(e_I(k)-D_k\cos\phi_k)^2 + (e_Q(k)-D_k\sin\phi_k)^2]\right\} \quad (54)$$

where $\sigma^2 = \text{var}[e_I(k)] = \text{var}[e_Q(k)]$. The envelope is $e(k) = [e_I^2(k) + e_Q^2(k)]^{0.5}$, where $e(k) \geq 0$. Defining a new variable $\theta(k) \triangleq \arctan[e_Q(k)/e_I(k)]$, $0 \leq \theta(k) \leq 2\pi$, $e_I(k)$ and $e_Q(k)$ may be written as functions of $e(k)$ and $\theta(k)$ as

$$e_I(k) = e(k)\cos\theta(k);$$
$$e_Q(k) = e(k)\sin\theta(k). \quad (55)$$

The joint probability density function of $e(k)$ and $\theta(k)$ given ϕ_k is

$$p(e(k),\theta(k)|\phi_k) = \frac{e(k)}{2\pi\sigma^2}\exp\left\{-\frac{1}{2\sigma^2}[e^2(k) + D_k^2 - 2D_k e(k)\cos(\phi_k - \theta(k))]\right\} \quad (56)$$

and

$$p(e(k)|\phi_k) = \int_0^{2\pi} p(e(k),\theta(k)|\phi_k)\,d\theta(k) = \frac{e(k)}{2\pi\sigma^2}\exp\left[-\frac{1}{2\sigma^2}(e^2(k)+D_k^2)\right] \times 2\pi I_0\left(\frac{D_k e(k)}{\sigma^2}\right) \quad (57)$$

where $I_0(x)$ is the modified Bessel function of zero order. This is independent of ϕ_k so that the density function of the envelope $e(k)$ is

$$p(e(k)) = \frac{e(k)}{\sigma^2}\exp\left[-\frac{1}{2\sigma^2}(e^2(k)+D_k^2)\right] I_0\left(\frac{D_k e(k)}{\sigma^2}\right). \quad (58)$$

The values of D_k and σ^2 under the H_1 and H_0 conditions are [11]

$$H_1 : D_1 = A(1-|\rho|)\text{sinc}[(\Delta\omega_d)N/2]$$
$$\sigma_1^2 = \left(\frac{N_0}{2}\right)\left\{1 + \left(\frac{C}{N_0}\right)\frac{T_s}{T_p}|\rho|^2 \times \text{sinc}^2[(\Delta\omega_d)N/2]\right\}/2N \quad (59)$$

$$H_0 : D_0 = 0$$
$$\sigma_0^2 = \left(\frac{N_0}{2}\right)\left\{1 + \left(\frac{C}{N_0}\right)\frac{T_s}{T_p}(1-2|\rho|+2|\rho|^2) \times \text{sinc}^2[(\Delta\omega_d)N/2]\right\}/2N. \quad (60)$$

If the threshold is set as D_t, then the detection probability is

$$P_d = \int_{D_t}^{\infty} p(e(k)|H_1)de(k). \quad (61)$$

Combining (58)–(59) and (61), (12) is derived. And the false-alarm probability is

$$P_{FA} = \int_{D_t}^{\infty} p(e(k)|H_0)de(k). \quad (62)$$

From (58), (60), and (62), (13) is obtained.

REFERENCES

[1] Wells, D., Beck, N., Delikaraoglou, D., Kleusberg, A., Krakiwsky, E. J., Lachapelle, G., Langley, R. B., Nakiboglu, M., Schwarz, K., Tranquilla, J. M., and Vanicek, P. (1986) *Guide to GPS Positioning.* Canadian GPS Associates, Fredericton, NB, 1986.

[2] Sage, C. F. (1964) Serial synchronization of pseudonoise systems. *IEEE Transactions on Communications*, **COM-12** (Dec. 1964), 123–127.

[3] Hopkins, P. M. (1980) A unified analysis of pseudonoise synchronization by envelope correlation. *IEEE Transactions on Communications*, **COM-28** (Aug. 1980), 1382–1388.

[4] Dicarlo, D. M., and Weber, C. L. (1983) Multiple dwell serial search: Performance and application to direct sequence code acquisition. *IEEE Transactions on Communications*, **COM-31**, 5 (May 1983), 650–659.

[5] Polydoros, A., and Weber, C. L. (1984) A unified approach to serial search spread-spectrum code acquisition, Part I and II. *IEEE Transactions on Communications*, **COM-32**, 5 (May 1984), 542–560.

[6] Spilker, J. J., Jr. (1963)
Delay-lock tracking of binary signals.
IEEE Transactions on Space Electronics Telemetry, **SET-9** (Mar. 1963), 1–8.

[7] Gill, W. J. (1966)
A comparison of binary delay-lock loop implementations.
IEEE Transactions on Aerospace and Electronic Systems, **AES-2** (July 1966), 415–424.

[8] Polydoros, A., and Weber, C. L. (1985)
Analysis and optimization of correlative code-tracking loops in spread-spectrum systems.
IEEE Transactions on Communications, **COM-33** (Jan. 1985), 30–43.

[9] Ziemer, R. E., and Peterson, R. L. (1985)
Digital Communications and Spread Spectrum Systems.
New York: Macmillan, 1985.

[10] Zhuang, W., and Tranquilla, J. (1993)
Digital baseband processor for the GPS receiver—Modeling and simulations.
IEEE Transactions on Aerospace and Electronic Systems, **AES-29**, 4 (Oct. 1993), 1343–1349.

[11] Zhuang, W. (1992)
Composite GPS receiver modeling, simulations and applications.
Ph.D. dissertation, Department of Electrical Engineering, University of New Brunswick, Fredericton, Canada, Oct. 1992.

[12] Papoulis, A. (1984)
Probability, Random Variables and Stochastic Processes (2nd ed.).
New York: McGraw-Hill, 1984, ch. 3.

[13] Lindholm, J. H. (1968)
An analysis of pseudo-randomness properties of subsequences of long m sequences.
IEEE Transactions on Information Theory, **IT-14** (July 1968), 569–576.

[14] Oppenheim, A. V., and Schafer, R. W. (1975)
Digital Signal Processing.
Englewood Cliffs, NJ: Prentice-Hall, 1975.

[15] Gill, W. J., and Spilker, Jr., J. J. (1963)
An interesting decomposition property for the self-products of random or pseudorandom binary sequences.
IEEE Transactions on Communications Systems, June 1963.

[16] Polydoros, A., and Pronios, N. B. (1988)
On the power density of digital modulated signals and applications in code despreading.
In *Proceedings of MILCOM'88*, Sept. 1988, 977–981.

Weihua Zhuang (M'93) received the B.Sc. (1982) and M.Sc. (1985) degrees from Dalian Marine University, China, and the Ph.D. degree (1993) from the University of New Brunswick, Canada, all in electrical engineering.

From January 1992 to September 1993, she was a Post Doctoral Fellow first at the University of Ottawa and then at Telecommunications Research Labs (TRLabs, Edmonton). Since October 1993, she has been with the Department of Electrical and Computer Engineering, University of Waterloo, Ontario, Canada, where she is an Assistant Professor. Her research interests include radio positioning and wireless digital communications.

James Tranquilla (S'69—M'77—SM'86) was born in New Brunswick, Canada in 1948 and received his degrees from the University of New Brunswick (B.Sc.E., M.Sc.E.) and University of Toronto (Ph.D.), all in electrical engineering.

Since 1976 he has been a faculty member at the University of New Brunswick where he is currently a Professor in the Electrical Engineering department.

Dr. Tranquilla has published over 150 papers and technical presentations in the research area of antennas and propagation, with applications in satellite navigation and EMI/EMC. He has acted as consultant to several international corporate and government clients in these areas and has formed both private and public companies offering professional engineering and technical services for the commercialization of new technologies.